THE JOURNAL OF PHYSICAL CHEMISTRY C

Article

pubs.acs.org/JPCC

Single-Walled Carbon Nanotubes Modulate the B- to A-DNA Transition

Gavin Bascom and Ioan Andricioaei*

Department of Chemistry, University of California, Irvine, California 92617, United States

ABSTRACT: We study the conformational equilibrium between B-to-A forms of ds-DNA adsorbed onto a single-walled carbon nanotube (SWNT) using free energy profile calculations based on all-atom molecular dynamics simulations. The potential of mean force (PMF) of the B-to-A transition of ds-DNA in the presence of an uncharged (10,0) carbon nanotube for two dodecamers with poly-AT or poly-GC sequences is calculated as a function of a root-mean-square-distance (ΔRMSD) difference metric for the B-to-A transition. The calculations reveal that in the presence of a SWNT DNA favors B-form DNA significantly in both poly-GC and poly-AT sequences. Furthermore, the poly-AT DNA:SWNT complex shows a higher energy penalty for adopting an A-like conformation than poly-GC DNA:SWNT by several kcal/mol. The presence of a SWNT on either poly-AT or poly-GC DNA affects the PMF of the transition such that the B form is favored by as much as 10 kcal/mol. In agreement with published data, we find a potential energy minimum between A and B-form DNA at ΔRMSD ≈ −1.5 Å and that the presence of the SWNT moves this minimum by as much as ΔRMSD = 3 Å.

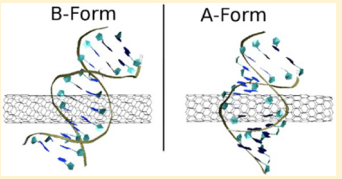

1. INTRODUCTION

The interaction of single-walled carbon nanotubes (SWNTs) with DNA is central to a variety of promising applications. In the field of nanotechnology, SWNT:DNA complexes are being used to construct nanoscale devices or nanosized building blocks with potential uses in the development of nanosize switches and nanoscale wiring.[1−3] In the realm of biotechnology, modulating the DNA:SWNT interaction can lead to applications such as SWNT purification, DNA recognition, and ultrafast DNA sequencing.[4−8] DNA:SWNT complexes also play an important role in cancer therapy and drug delivery.[9] Because the DNA structure influences the physical properties of the devices used in these applications (such as their electrical, spectroscopic, or thermal properties) and because DNA is known to change its local or global structure upon binding to macromolecules, it is important to assess how SWNT adsorption modulates the conformational details of DNA. For example, the interplay between the A and B forms of DNA[10] plays roles in several biological processes (the transition from the B-DNA double helix to the A-form is essential for biological function, as DNA is in the A-form in many protein−DNA complexes). Specifically, B-DNA describes an ensemble of conformers which prevail for free DNA under physiological conditions,[11] while A-form DNA has been found complexed with various ligands and proteins and is commonly seen in synthetic DNA complexes or partially dehydrated DNA complexes.[12,13] Elucidation of the details involving secondary structure behavior in different environments is particularly important when discussing DNA rigidity and the tendency to bend in a sequence-specific manner.[14]

Molecular dynamics (MD) simulations have been able to accurately describe how both single-stranded DNA (ss-DNA) and double-stranded DNA (ds-DNA) interacts with nanotube-like objects. In the case of ss-DNA, Goa et al.[15] show in a set of atomistic simulations that the ss-DNA adsorbs quickly to the surface of the SWNT or inserts into the interior of a SWNT depending on the size of the tube. These "binding" modes have also been verified experimentally.[16] In the case of double-stranded DNA (ds-DNA), simulations show that ds-DNA can also enter the interior of SWNTs in stable conformations[17] or can bind a SWNT in the major groove of the DNA helix. Electronic structure calculations of ds-DNA with a SWNT placed in the major groove were used to predict a stable binding conformation.[7] In a study by Zhoa and Johnson,[18] ds-DNA was simulated by MD and shown to adsorb to the surface of SWNTs in various conformations depending on the charge of the nanotube; these direct simulations of the binding event occurred on a time scale on the order of nanoseconds. In the case of an uncharged SWNT, the adsorbed ds-DNA was found to adopt a hybrid A/B secondary structure form in which certain features of A-form DNA could be seen but B-form elements remained as well. In contrast, a positively or negatively charged SWNT:DNA complex favored the B-form in a Dickerson−Drew dodecamer (sequence d-$[CGCGAATTCGCG]_2$). While this study is one of the few studies published on ds-DNA secondary structure in the presence of SWNTs, it leaves several questions unanswered regarding the range of B-to-A forms when SWNTs are present particularly since the time scale of the simulations was short relative to the typical DNA structural relaxation times.

The dynamics of the B-to-A transition is subject to different interpretations.[19] According to molecular dynamics simulations, the transition from one state in the external conditions conducive to the other state is expected to occur over several

Special Issue: John C. Hemminger Festschrift

Received: August 11, 2014
Revised: October 20, 2014
Published: October 21, 2014

   dx.doi.org/10.1021/jp5081274 | J. Phys. Chem. C 2014, 118, 29441−29447

nanoseconds. The B-to-A transition in stopped flow experiments on the other hand is complete over times with an upper bound of 0.2 ms. When the reaction was followed with an electric field jump technique (which induced the transition by a driving force involving dipole stretching from A to B), a cooperative transition on the time scale of 10 μs was observed.

Altogether, the experimental data suggest the existence of an activation barrier for the B-to-A transition, with clearly separated helical states. In contrast, the molecular dynamics simulations point to a view in which, rather than well-separated states, the A-DNA and B-DNA descriptors delimit a continuum whose equilibrium populations are modulated by a smooth free energy profile between two intermediates. This profile is further modulated by relatively small variations in external conditions (although, interestingly, under the salt conditions used for the experimental studies of the B-to-A transition, the relaxation times were almost independent of the ionic strength). For example, Ho et al.[20] used X-ray crystallography to characterize the trapped DNA hexamer GGCGCC in various states straddling A- and B-form DNA. These can be induced not only by chemical modifications of cytosine but also by crystal packing.[21] Because of the fine role of DNA structure in modulating binding affinities, it is important to ask what are the effects of carbon nanotubes in the transition between A and B forms, and how we may further exploit that role for further use.

It is of value to assess precisely the details of the B−A equilibrium and interconversion since nanotechonology applications are likely to depend on the intimate details of DNA fine structure, such as base stacking, major−minor groove access, or sugar−phosphate backbone structure. They are relevant because the DNA−nanotube interaction modulates the applications through the details that the chemical and electrical properties of DNA:SWNT complexes offer to nanoscale devices, along with the ability to manipulate the DNA sequence. The A-form DNA double helix is wider and shorter than the B-form helix. Its base pairs are tilted relative to the helical axis in the A form, while they are perpendicular to the helix axis in B-DNA. Moreover, the stacking of bases in A-DNA is substantially different than in B-DNA, and the major groove of A-DNA is narrower and deeper (see Figure 1). These structural differences will modulate the physicochemical properties of interest. Moreover, a particular question is also whether the base sequence has any effect on the transition between B and A forms.

Here, we compute the free energy profile along an order parameter based on root-mean-square-distance (RMSD) differences, a coordinate that spans the B-to-A transition in two poly-AT or poly-GC dodecamers using umbrella sampling MD simulations[22] and the weighted histogram analysis method (WHAM)[23] in the presence of an uncharged 10,0 SWNT.

For free ds-DNA, the B-to-A transition has been studied in terms of free energy considerations using umbrella sampling and the weighted histogram analysis method.[10,24] Our study herein addresses the B-to-A transition of DNA in the presence of a bound SWNT in atomistic detail, providing insight into the DNA:SWNT binding mode and the degree of the conformational change that the nanotube adsorption induces. We report a quantitative estimate of the energy involved in the B-to-A transition. Such calculations are important, for example, in the context of recent work concerning optical spectroscopy,[25,26] in which geometric and energetic estimates of DNA adsorption were used to calculate band gap fluorescence and provide details for SWNT:DNA based experimental assays, in both liquid blood and dense tissues.

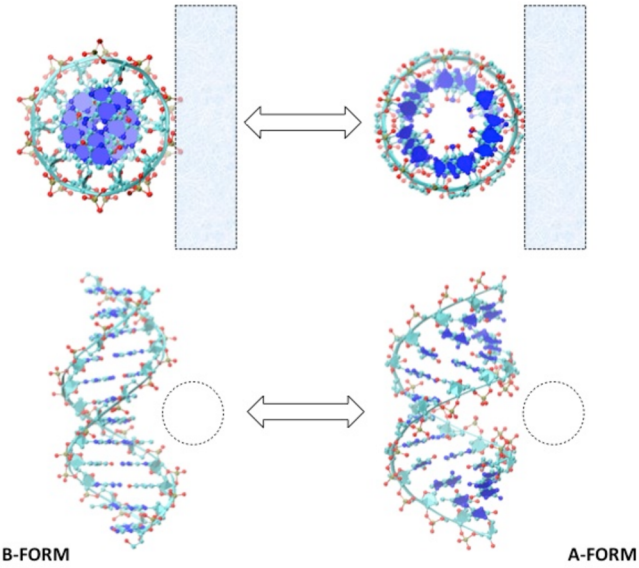

Figure 1. Ideal B- and A-form DNA shown from the top and side, with the outline of the SWNT position during simulations. Note the widening of the interhelical distance and major groove upon converting from B to A form. Double arrows indicate interconversion in a smooth continuous fashion as a response to environmental changes.

2. COMPUTATIONAL METHODS

Four systems, namely, A- and B-form poly-GC and poly-AT DNA molecules, were generated using the Nucleic Acid Builder (NAB) software package,[27] and the SWNT was generated using TubeGen 3.3.[3,28] The systems were solvated via visual molecular dynamics (VMD),[29] with 22 Na^+ ions and TIP3P[30] water to neutralize charge and represent solvent explicitly with cubic water boxes 80 Å on each side generated within the MMTSB modeling package[31] using the CHARMM29 force field.[32,33] Short-range electrostatics were truncated at 12 Å with a switching function beginning at 10 Å, while long-range electrostatics were calculated with the particle mesh Ewald method[34] with a grid spacing of 1.0 Å and a sixth-order B-spline used for interpolation. A 2 fs time step was employed with the SHAKE[35] algorithm as implemented in CHARMM to constrain bonds to hydrogens. The SWNT was placed initially in the same configuration relative to the DNA as that calculated in the study by Lu et al.[7] (shown in Figure 2), who used a self-consistent charge density-functional-based tight-binding method (SCC-DFTB)[36] to determine energetics, relative stability, and electronic properties of the complexed system.

Each system was minimized and then heated using Langevin dynamics and equilibrated for 2 ns, with harmonic constraints placed on heavy atoms for initial heating and released when the systems completed the equilibration phase. Harmonic constraints were then placed on all carbon atoms of the SWNT to hold them in their equilibrated positions, while another harmonic constraint held the distance between the DNA center of mass and the SWNT center of mass stable. We adopted the ΔRMSD metric as our order parameter similar to work done previously by Banavali and Roux,[24] wherein the metric was used to study the energetics of B- to A-form DNA transitions. ΔRMSD is defined as the difference between the

dx.doi.org/10.1021/jp5081274 | J. Phys. Chem. C 2014, 118, 29441−29447

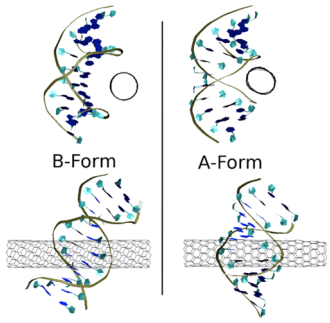

Figure 2. Absorbed SWNT on ds-DNA shown from side and front view, in the A and B form. The DNA binds the SWNT in the major groove; conformation used from calculations in ref 7.

RMSDs of an instantaneous structure relative to two reference structures (the B and the A forms) (see below). This metric is advantageous as a reaction coordinate for smooth transitions because it neither forces the system along one particular reaction pathway nor biases it toward one reference in particular, but still retains the convenience of a single-order parameter around which one can constrain with simple harmonic potentials. In other words, the reaction coordinate structures are allowed to move around in sample space away from the two end structures, as long as the difference between RMSD (relative to the end points) is harmonically restrained in successive i-labeled umbrella potentials according to the restraint potential energy

$$V_i(\vec{r}) = k^i[\Delta\rho(\vec{r}) - \Delta\rho^i_{\min}]^2 \quad (1)$$

where k^i is the harmonic force constant of the ith restraint and

$$\Delta\rho(\vec{r}) = \mathrm{RMSD}_B(\vec{r}) - \mathrm{RMSD}_A(\vec{r}) = \Delta\mathrm{RMSD}(\vec{r}) \quad (2)$$

with $\vec{r}$ being the $3N$-dimensional configurational vector of the N atoms in the system, and $\mathrm{RMSD}_B = \|\vec{r} - \vec{r}_B\|$ and $\mathrm{RMSD}_A = \|\vec{r} - \vec{r}_A\|$ where $\|\cdots\|$ denotes the 2-norm of the difference of the Cartesian coordinates of an instantaneous configuration $\vec{r}$ with respect to idealized A- or B-form Cartesian coordinates. In this way we apply a restraining force involving both A and B forms as reference structures, using k^i as the force constant and $\Delta\rho^i_{\min}$ as the minimum around which we constrain the reaction coordinate in the i-th simulation window. The reaction coordinate $\Delta\rho$ is chosen such that it is a (positive) maximum if the system is in an A-like conformation, whereas $\Delta\rho$ is a minimum (negative) when the system is in a B-like conformation (although degenerate extrema in $\Delta\rho$ exist for non-A or -B forms, according to the geometry of the underlying multidimensional hyperboloids involved in the definition of the order parameter). Employing our constraint, $\Delta\rho$ was restrained from −5 to 5 Å with windows of 0.4 Å spacing. Each umbrella sampling window was equilibrated for 1 ns, and each window was initiated from the final coordinates of the previous window to minimize the value of the energy penalty due to our constraint from window to window. ΔRMSD for each window was binned as a histogram, and sufficient overlap between neighboring windows was accumulated as needed to achieve convergence of the PMF, which was calculated using the WHAM method.[23,37] The autocorrelation function (ACF) of our reaction coordinate $\Delta\rho$ across simulation time t, $C(t) = \langle\Delta\rho(0)\cdot\Delta\rho(t)\rangle$ was fitted to a single exponential $e^{-t/\tau}$. The decay time τ was found to be within a tenth of our simulation time, ensuring convergence of the metric and allowing for bootstrap error analysis within the WHAM implementation.[23,37] Although necessary but not sufficient conditions for accuracy, error margins were found to be small enough to be considered negligible (data not shown). Furthermore, once the PMF was calculated, additional windows were run at regular intervals and intercalated between each previously run window (bringing total window separation to 2 Å), with little change observed in overall PMF curves, suggesting convergence of the calculation.

3. POTENTIAL OF MEAN FORCE

The free energy profile $F(\Delta\rho) = -k_B T \ln\langle P(\Delta\rho)\rangle$ is the potential of mean force[38] with respect to the RMSD difference reaction coordinate $\Delta\rho$. Its negative gradient is the average force it takes to hold the system at a given value of $\Delta\rho$. In our case, repeatedly restraining along the RMSD difference along predefined points with umbrella potentials and using the weighted histogram analysis method (WHAM), we calculated $F(\Delta\rho)$ along the B-to-A DNA transition. Figures 3 and 4 report

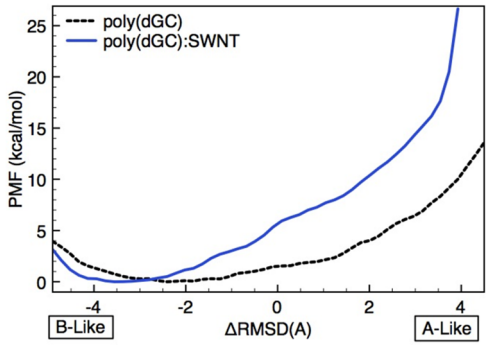

Figure 3. Potential of mean force curves generated for poly-GC DNA dodecamer with or without the presence of SWNT fitted into the major groove, plotted against the B-to-A transition gauged via $\Delta\mathrm{RMSD} = \mathrm{RMSD}_B - \mathrm{RMSD}_A$. A negative ΔRMSD represents large B character and little A character, whereas a positive ΔRMSD represents large A character and little B character. The free energy of binding to the SWNT is not included. The well in the bound state near B-like structures is more favored; i.e., along the same curve, B-like forms are favored, as in the case of free DNA.

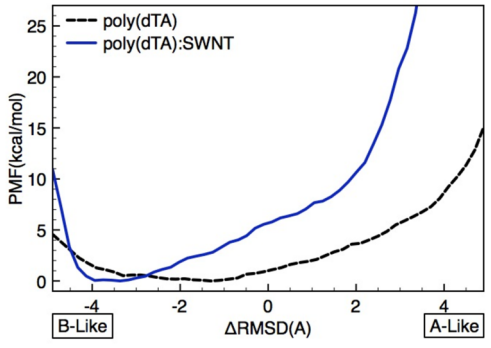

Figure 4. Potential of mean force curves generated for poly-TA DNA dodecamer with or without the presence of SWNT fitted into the major groove, plotted against the B-to-A transition. Systems with nanotubes present generated force profiles similar to those without SWNT but favor the B form by as much as 10 kcal/mol, with the poly-AT sequence being affected the most.

dx.doi.org/10.1021/jp5081274 | J. Phys. Chem. C 2014, 118, 29441−29447

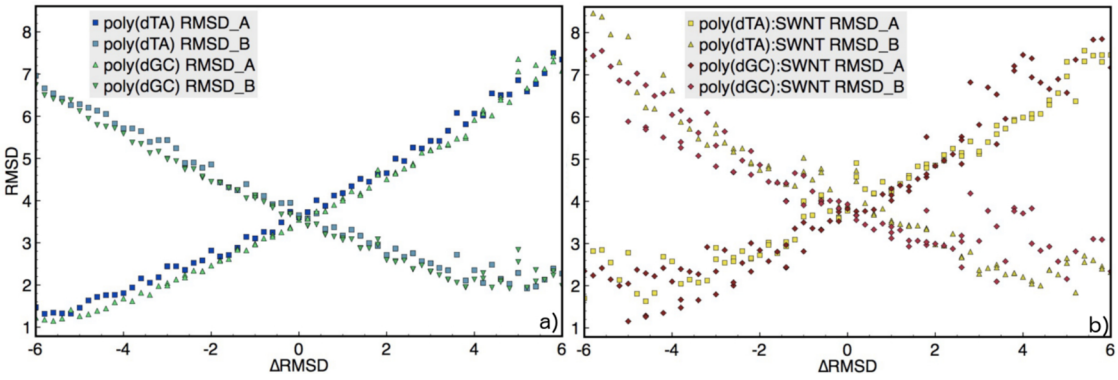

Figure 5. Averages of RMSD with respect to A and B structures for each window plotted against the position of the ΔRMSD constraint (b) with SWNT present and (a) with no SWNT present. A negative ΔRMSD represents large B character and little A character, whereas a positive ΔRMSD represents large A character and little B character. (a) Shows a smooth transition to A form without SWNT present, whereas (b) shows the difficulty that DNA has in adopting the A form despite the constraint being applied.

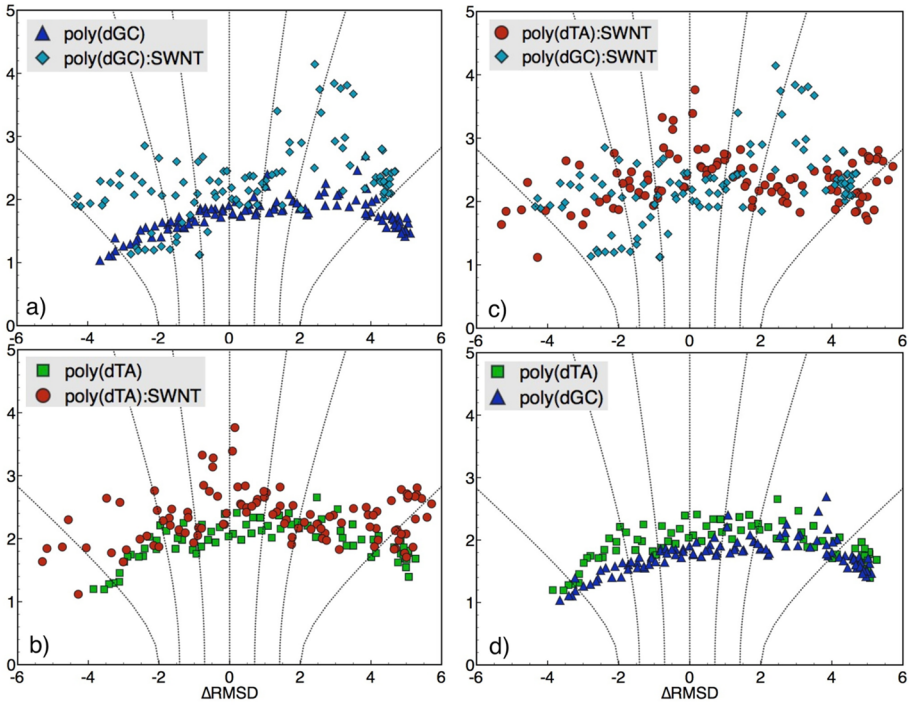

Figure 6. Average values of $RMSD_A$ and $RMSD_B$ for each window plotted against a contour plot of the hyperbolic constraint used for umbrella windows. The distance from each data point to the point (−3,0) represents $RMSD_A$, and $RMSD_B$ is represented by the distance to point (3,0). Several examples of the constraint windows are shown, representing 5 of the 100 windows used to bias sampling along the reaction coordinate ΔRMSD, which is plotted along the abscisa. Each of the hyperbolas plotted here represents the geometric locus of a constant difference between RMSDs relative to ideal A and B forms (which are the two foci of the hyperbolas), with the difference between A and B forms representing the distance between the foci (6 Å).

the resulting curves for the potential of mean force (in kcal/mol) generated for poly-AT and poly-GC DNA dodecamers with or without the presence of a SWNT fitted into the major groove plotted against $\Delta\rho = RMSD_B - RMSD_A$ in Å. As discussed above, a negative $\Delta\rho$ represents a large B character with little A character (or at least proximity in the RMSD difference), whereas a positive $\Delta\rho$ represents substantial A and little B character. Systems without the nanotube present generated force profiles with features similar to those generated by Banavali and Roux,[24] which are in accord with experimental results concerning the B-to-A transition. PMF curves generated with SWNT favor the B form by as much as ∼10 kcal/mol. This is significant at room temperature $k_BT \simeq 0.6$ kcal/mol, indicating that the duplexes have ∼2 Å of the well minimum available for fluctuations, a fact that is in good agreement with molecular simulation about RMSD fluctuation even at relatively short time scales.[14] The presence of the SWNT shifts the PMF minima in the negative ΔRMSD direction, indicating that more B-like fluctuations are likely available to both the poly-GC and the poly-AT dodecamers. Furthermore, Figure 4 shows that near AT-rich sequences this effect is felt in relative well height additionally, indicating that the fluctuations are even more B-like around AT-rich sequences. Additionally, we note the asymmetric nature of the free energy wells with respect to the midpoint between A and B forms, indicating that there is an anharmonic stiffness in response to the SWNT presence for

dx.doi.org/10.1021/jp5081274 | J. Phys. Chem. C 2014, 118, 29441−29447

both poly-GC and poly-AT sequences. For DNA without nanotubes present, this feature is in accord with previous simulations.[24] In the presence of the nanotubes, our results show that this asymmetry is further strengthened (cf. Figures 3 and 4).

We also report the individual RMSD measures with respect to the starting structure and both target structures along the sampled pathways in Figure 5 in order to describe the evolution of the individual RMSD components $RMSD_A$ and $RMSD_B$ throughout the simulation windows along the pathways. In Figure 6 we show the pathway overlaid over the (hyperbolic) cuts through the multidimensional hyperboloids which are the geometrical loci of constant RMSD difference (i.e., $\Delta\rho$) values. These plots show that the presence of the nanotube alters the free energy pathways connecting the A and B forms relative to the pathways in the absence of the nanotube.

4. CONCLUDING DISCUSSION

The results for the free energy profiles show a propensity for DNA to be in the B form in standard MD solvent with neutralizing ionic conditions and no SWNT structures present, which is consistent with both experiment and previous MD results. A physical instantiation of DNA:SWNT complexes with our particular geometry is relevant for assays showing DNA:SWNT adsorption without specific geometry elucidation (see ref 39). The geometry used herein has been shown to be a steady configuration when modeled using electronic structure calculations[7] and generated discussions in reference to several important biotechnology applications and nanodevices.[40] Our results suggest that the presence of the nanotube will influence the proximal DNA to be in B form, with some specificity between AT tracts and GC tracts. While the difference between poly-GC and poly-AT dodecamer energetics is only ∼10 kcal/mol, our evidence suggests that some difference in structure alone, perhaps rigidity or steric hindrances, makes for a substantial energy difference for A-to-B form transitions in a sequence-dependent way. While it may be tempting to attribute these sequence-dependent effects to specific attributes of A/T- or G/C-rich DNA, one must remember that the force fields employed herein are highly parametrized, and one should therefore only refer to simulated results which are experimentally corroborated. While these results suggest that experimentally mimicking this setup would result in observable sequence dependence, they do not allow the presumption of which fine-tuned details of sequence dependence would result in specific B-form stabilization. In fact, experimental validation of the free energy profiles calculated herein can be achieved with single-molecule correlates of free energy[41] obtained from repeated pulling experiments of the DNA−SWNT complex that can relate thermodynamics to the resulting force−extension profiles. Further applications can be envisioned to explore the unique properties of the SWNT−DNA interaction, which may lead to advances in fast gene sequencing techniques.[42]

The asymmetry of the free energy profiles we present in Figures 3 and 4 are pertinent in the framework set by the recent results of Mazur.[43] That study reported an *asymmetric* response of DNA to local twist in simulation. While, as discussed above, this anharmonicity exists for naked DNA, it is further enhanced by the presence of the nanotube. With SWNT adsorbed, the DNA somewhat unwinds its double helix against the helical "grain" from the A form (which is shorter and wider) to the B form (more elongated and narrower). Such an asymmetry in the twisting of DNA is in agreement with the calculations of the anharmonic torsional stiffness of DNA under small external torques observed by Mazur.[43] Our free energy profiles also show that for the same span or ΔRMSD going from B to A, there is significantly larger resilience of SWNT-adsorbed DNA with AT sequence relative to that of the GC, by ∼10 kcal/mol for the former relative to the latter form (cf. Figures 3 and 4). Keeping in mind that the nanotube is largely hydrophobic, this also recapitulates results for decreasing levels of DNA hydration. According to that study,[43] while the dynamics of the B-to-A transition in dodecameric poly(dA)−poly(dT) is smooth and easy to achieve upon decreasing water content in the simulations, for poly(dG)−poly(dC), which are also known from experiment to exhibit contrasting properties, the B−A transition of the dodecamer fragment could not be obtained even though the A-DNA form is known to be stable in low hydration conditions. In biophysical terms, a major contribution to the forces present in the DNA−SWNT interaction involves the attraction of the hydrophobic surface of the SWNT to the hydrophobic moieties of the bases. In the case of the uncharged SWNT simulated here, it is difficult to estimate the major influence this force imparts on the DNA on the scale of long sequences. The overall role of water is clearly another relevant aspect of the current discussion, but without an exact experimental corroboration with the simulated system setup it may be very difficult to fully characterize that role with simulation alone. Further investigation should be made to attempt to fully characterize the role of hydration and ionic effects in DNA:SWNT complexes and DNA in different electronic environments.

Our results suggest, however, that these effects manifest at least in part as a propensity to favor B DNA locally, particularly near AT-rich sequences. While a further study regarding a larger number of sequences would be interesting, it would require an unfeasibly large number of sequence permutations compared to our limited two-sequence study. A complicating aspect is also that for mixed sequences it may not be clear what the sequence effect will be, as flanking steps are numerous (e.g., CG:CG vs CG:GC vs CG:AT etc.). Sequence permutation provides an interesting search space, however, and perhaps this initial work will inspire further experimental and theoretical study in the future. Furthermore, interpretation of specific effects of sequence change would likely require very subtle experimental backing for validation. For example, the specific effects of heterogeneous sequences on backbone rigidity were recently shown—by MD simulation and S^2 NMR order parameter measurements—to have a significant role in DNA dynamics,[14] a conclusion which is likely at play in explaining sequence dependence. More details regarding individual contributions of backbone rigidity versus base coupling energies may also be explored by repeating these calculations using ds-RNA as opposed to ds-DNA, which favors A conformations generally.

Furthermore, our PMF curves are in agreement with published results regarding sequence dependence, specifically in their ability to reproduce the slight bend seen around adenine-thymine tracts in solution.[44,45] It has been shown that AT heavy sequences (such as the ones studied herein) show slight bends toward the A conformation. Moreover, the energies involved match well with those computed theoretically from such bending, with values ∼5 kcal/mol.[45,46] As mentioned, while the sequences investigated herein are rather limited, further work should be carried out in both experiment

dx.doi.org/10.1021/jp5081274 | J. Phys. Chem. C 2014, 118, 29441−29447

and simulation to further characterize the more subtle effects of sequence-dependent DNA stiffness in different electronic environments. Furthermore, it would be important to determine if sequence-specific stabilization is dependent on a simple base composition ratio or if specifically designed sequences could be stabilized by nanotube presence.

Taken together, all these data suggest that DNA has the inherent ability to resist twisting and stacking rearrangements simply by virtue of short *sequence*-mediated local conformational changes. Remarkably, the presence on carbon nanotubes of the type simulated here accentuate this modulation, suggesting that their presence can modulate B-to-A conformational changes in a cellular context, for example, when proteins bind DNA. Further conformational studies of SWNT binding of longer DNA duplexes of more diverse sequences may aid in revealing further details of conformational properties and local reorganization in DNA−carbon nanotube systems.

AUTHOR INFORMATION

Corresponding Author

*Phone: (949) 824-3569. E-mail: andricio@uci.edu.

Notes

The authors declare no competing financial interest.

ACKNOWLEDGMENTS

GB thanks the National Science Foundation for generous allocation of resources at Teragrid Computing Center and the University of California Irvine. IA acknowledges support from NIH grant 5R016M089846.

REFERENCES

(1) Kong, J.; Franklin, N. R.; Zhou, C.; Chapline, M. G.; Peng, S.; Cho, K.; Dai, H. Nanotube Molecular Wires as Chemical Sensors. *Science* **2000**, *287*, 622−625.

(2) Wang, J. Nanomaterial-Based Electrochemical Biosensors. *Analyst* **2005**, *130*, 421−426.

(3) Dresselhaus, M. S.; Dresselhaus, G.; Eklund, P. C. *Science of Fullerenes and Carbon Nanotubes: Their Properties and Applications*; Academic Press: New York, 1996.

(4) Hahm, J.; Lieber, C. Direct Ultrasensitive Electrical Detection of DNA and DNA Sequence Variations Using Nanowire Nanosensors. *Nano Lett.* **2004**, *4*, 51−54.

(5) Santos, A.; Barone, P.; Chou, S.; Diner, B. Structure-Based Carbon Nanotube Sorting by Sequence-Dependent DNA Assembly. *Science* **2003**, *302*, 1545−1548.

(6) Williams, K. A.; Veenhuizen, P. T. M.; de la Torre, B. G.; Eritja, R.; Dekker, C. Nanotechnology: Carbon Nanotubes with DNA Recognition. *Nature* **2002**, *420*, 761.

(7) Lu, G.; Maragakis, P.; Kaxiras, E. Carbon Nanotube Interaction with DNA. *Nano Lett.* **2005**, *5*, 897−900.

(8) Meng, S.; Maragakis, P.; Papaloukas, C. DNA Nucleoside Interaction and Identification with Carbon Nanotubes. *Nano Lett.* **2007**, *7*, 45−50.

(9) Nie, S.; Xing, Y.; Kim, G.; Simons, J. Nanotechnology Applications in Cancer. *Annu. Rev.* **2007**, *9*, 257−288.

(10) Noy, A.; Perez, A.; Laughton, C. A.; Orozco, M. Theoretical Study of Large Conformational Transitions in DNA: the B A Conformational Change in Water and Ethanol/Water. *Nucleic Acid Res.* **2007**, *35*, 3330−3338.

(11) Baianu, I. C. Structural Order and Partial Disorder in Biological Systems. *Bull. Mater. Biol.* **1980**, *42*, 137−141.

(12) Wahl, M. C.; Sundaralingam, M. Crystal Structures of A-DNA Duplexes. *Biopolymers* **1997**, *44*, 45−63.

(13) Lu, X.-J.; Shakked, Z.; Olson, W. K. A-Form Conformational Motifs in Ligand-bound DNA Structures. *J. Mol. Biol.* **2000**, *300*, 819−840.

(14) Nikolova, E.; Bascom, G.; Andricioaei, I.; Al-Hashimi, H. Probing Sequence-specific DNA Flexibility in A-tracts and Pyrimidine-purine Steps by Nuclear Magnetic Resonance 13C Relaxation and Molecular Dynamics Simulations. *Biochemistry* **2012**, *51*, 8654−8664.

(15) Gao, H.; Kong, Y. Simulation of DNA-nanotube Interactions. *Annu. Rev. Mater. Res.* **2004**, *34*, 123−150.

(16) Okada, T.; Kaneko, T.; Hatakeyama, R.; Tohji, K. Electrically Triggered Insertion of Single-stranded DNA into Single-walled Carbon Nanotubes. *Chem. Phys. Lett.* **2006**, *417*, 288−292.

(17) Lau, E.; Lightstone, F.; Colvin, M. Dynamics of DNA Encapsulated in a Hydrophobic Nanotube. *Chem. Phys. Lett.* **2005**, *412*, 82−87.

(18) Zhao, X.; Johnson, J. K. Simulation of Adsorption of DNA on Carbon Nanotubes. *J. Am. Chem. Soc.* **2007**, *129*, 10438−10445.

(19) Jose, D.; Porschke, D. Dynamics of the BA Transition of DNA Double Helices. *Nucleic Acid Res.* **2004**, *32*, 2251−2258.

(20) Vargason, J. M.; Henderson, K.; Ho, P. S. A Crystallographic Map of the Transition from B-DNA to A-DNA. *Proc. Natl. Acad. Sci. U.S.A.* **2001**, *98*, 7265−7270.

(21) Dickerson, R. E.; Ng, H. L. DNA Structure From A to B. *Proc. Natl. Acad. Sci. U.S.A.* **2001**, *98*, 6986−8.

(22) Torrie, G. M.; Valleau, J. P. Non-Physical Sampling Distributions in Monte-Carlo Free-energy Estimation - Umbrella Sampling. *J. Comput. Phys.* **1977**, *23*, 187−199.

(23) Kumar, S.; Bouzida, D.; Swendsen, R.; Kollman, P.; Rosenberg, J. The Weighted Histogram Analysis Method for Free-energy Calculations on Biomolecules. I. The Method. *J. Comput. Chem.* **1992**, *13*, 1011−1021.

(24) Banavali, N. K.; Roux, B. Free Energy Landscape of A-DNA to B-DNA Conversion in Aqueous Solution. *J. Am. Chem. Soc.* **2005**, *127*, 6866−76.

(25) Barone, P. W.; Baik, S.; Heller, D. A.; Strano, M. S. Near-infrared Optical Sensors Based on Single-walled Carbon Nanotubes. *Nat. Mater.* **2005**, *4*, 86−92.

(26) Heller, D. A.; Baik, S.; Eurell, T. E.; Strano, M. S. Single-Walled Carbon Nanotube Spectroscopy in Live Cells: Towards Long-Term Labels and Optical Sensors. *Adv. Mater.* **2005**, *17*, 2793−2799.

(27) Case, D.; Darden, T.; Cheatham Iii, T.; Simmerling, C.; Wang, J.; Duke, R.; Luo, R.; Walker, R.; Zhang, W.; Merz, K.; et al. *Amber Tools 1.5*; 2010.

(28) Frey, J. T.; Doren, D. J. *Tubegen 3.3*, http://turin.nss.udel.edu/research/tubegenonline.html, 2005.

(29) Humphrey, W.; Dalke, A.; Schulten, K. VMD: Visual Molecular Dynamics. *J. Mol. Graphics* **1996**, *14*, 33−38.

(30) Jorgensen, W. L.; Jenson, C. Temperature Dependence of TIP3P, SPC, and TIP4P Water from NPT Monte Carlo Simulations: Seeking Temperatures of Maximum Density. *J. Comput. Chem.* **1998**, *19*, 1179−1186.

(31) Chocholousová, J.; Feig, M. Implicit Solvent Simulations of DNA and DNA-Protein Complexes: Agreement with Explicit Solvent vs Experiment. *J. Phys. Chem. B* **2006**, *110*, 17240−51.

(32) Brooks, B. R.; Bruccoleri, R. E.; Olafson, B. D.; States, D. J.; Swaminathan, S.; Karplus, M. CHARMM: A Program for Macromolecular Energy, Minimization, and Dynamics. *J. Comput. Chem.* **1983**, *4*, 187−217.

(33) MacKerrell, A. D.; Karplus, M. All-Atom Empirical Potential for Molecular Modeling and Dynamics Studies of Proteins. *J. Phys. Chem. B* **1998**, *102*, 3586−3616.

(34) Darden, T.; York, D.; Pedersen, L. Particle Mesh Ewald: An Nlog(N) method for Ewald Sums in Large Systems. *J. Chem. Phys.* **1993**, *98*, 10089−10092.

(35) Ryckaert, J.-P.; Ciccotti, G.; Berendsen, H. J. Numerical Integration of the Cartesian Equations of Motion of a System with Constraints: Molecular Dynamics of *n*-Alkanes. *J. Comput. Phys.* **1977**, *23*, 327−341.

(36) Elstner, M.; Porezag, D.; Jungnickel, G.; Elsner, J.; Haugk, M.; Frauenheim, T.; Suhai, S.; Seifert, G. Self-Consistent-Charge Density-Functional Tight-Binding Method for Simulations of Complex Materials Properties. *Phys. Rev. B* **1998**, *58*, 7260.
(37) Roux, B. The Calculation of the Potential of Mean Force Using Computer Simulations. *Comput. Phys. Commun.* **1995**, *13*, 1011−1021.
(38) Kirkwood, J. Statistical Mechanics of Fluid Mixtures. *J. Chem. Phys.* **1935**, *3*, 300−313.
(39) Star, A.; Tu, E.; Niemann, J.; Gabriel, J.-C. P.; Joiner, C. S.; Valcke, C. Label-free detection of DNA hybridization using carbon nanotube network field-effect transistors. *Proc. Natl. Acad. Sci. U.S.A.* **2006**, *103*, 921−926.
(40) Daniel, S.; Rao, T. P.; Rao, K. S.; Rani, S. U.; Naidu, G.; Lee, H.-Y.; Kawai, T. A Review of DNA Functionalized/Grafted Carbon Nanotubes and their Characterization. *Sensors Actuators, B: Chem.* **2007**, *122*, 672−682.
(41) Keller, D.; Swigon, D.; Bustamante, C. Relating Single-molecule Measurements to Thermodynamics. *Biophys. J.* **2003**, *84*, 733−738.
(42) Lu, D.; Aksimentiev, A.; Shih, A. Y.; Cruz-Chu, E.; Freddolino, P. L.; Arkhipov, A.; Schulten, K. The Role of Molecular Modeling in Bionanotechnology. *Phys. Biol.* **2006**, *3*, S40.
(43) Mazur, A. K. Anharmonic Torsional Stiffness of DNA Revealed Under Small External Torques. *Phys. Rev. Lett.* **2010**, *105*, 018102.
(44) Hizver, J.; Rozenberg, H.; Frolow, F.; Rabinovich, D.; Shakked, Z. DNA bending by an Adenine-Thymine Tract and its Role in Gene Regulation. *Proc. Natl. Acad. Sci. U.S.A.* **2001**, *98*, 8490−5.
(45) Koo, H. S.; Drak, J.; Rice, J. A.; Crothers, D. M. Determination of the Extent of DNA Bending by an Adenine-Thymine Tract. *Biochemistry* **1990**, *29*, 4227−34.
(46) Curuksu, J.; Zacharias, M.; Lavery, R.; Zakrzewska, K. Local and Global Effects of Strong DNA Bending Induced During Molecular Dynamics Simulations. *Nucleic Acid Res.* **2009**, *37*, 3766−3773.